CORA Cork Open Research Archive
Cartlann Taighde Oscailte Chorcaí

Title	Enhanced mass activity and stability of bimetallic Pd-Ni nanoparticles on boron-doped diamond for direct ethanol fuel cell applications
Authors	Mavrokefalos, Christos K.;Hasan, Maksudul;Rohan, James F.;Foord, John S.
Publication date	2017-11-20
Original Citation	Mavrokefalos, C. K., Hasan, M., Rohan, J. F. and Foord, J. S. (2017) 'Enhanced mass activity and stability of bimetallic Pd-Ni nanoparticles on boron-doped diamond for direct ethanol fuel cell applications', ChemElectroChem, 5(3), pp. 455-463. doi:10.1002/celc.201701105
Type of publication	Article (peer-reviewed)
Link to publisher's version	10.1002/celc.201701105
Rights	© 2017, John Wiley & Sons, Inc. This is the peer reviewed version of the following article: Mavrokefalos, C. K., Hasan, M., Rohan, J. F. and Foord, J. S. (2017) 'Enhanced mass activity and stability of bimetallic Pd-Ni nanoparticles on boron-doped diamond for direct ethanol fuel cell applications', ChemElectroChem, 5(3), pp. 455-463, doi:10.1002/celc.201701105. This article may be used for non-commercial purposes in accordance with Wiley Terms and Conditions for Self-Archiving.
Download date	2026-11-05 17:36:57
Item downloaded from	https://hdl.handle.net/10468/5179

UCC
University College Cork, Ireland
Coláiste na hOllscoile Corcaigh

FUNDAMENTALS & APPLICATIONS

CHEMELECTROCHEM

ANALYSIS & CATALYSIS, BIO & NANO, ENERGY & MORE

Accepted Article

Title: Enhanced Mass Activity and Stability of Bimetallic Pd-Ni Nanoparticles on Boron-Doped Diamond for Direct Ethanol Fuel Cell Applications

Authors: Christos K Mavrokefalos, Maksudul Hasan, James F Rohan, and John S Foord

This manuscript has been accepted after peer review and appears as an Accepted Article online prior to editing, proofing, and formal publication of the final Version of Record (VoR). This work is currently citable by using the Digital Object Identifier (DOI) given below. The VoR will be published online in Early View as soon as possible and may be different to this Accepted Article as a result of editing. Readers should obtain the VoR from the journal website shown below when it is published to ensure accuracy of information. The authors are responsible for the content of this Accepted Article.

To be cited as: *ChemElectroChem* 10.1002/celc.201701105

Link to VoR: http://dx.doi.org/10.1002/celc.201701105

A Journal of

ChemPubSoc Europe

WILEY-VCH

www.chemelectrochem.org

WILEY-VCH

ARTICLE

Enhanced Mass Activity and Stability of Bimetallic Pd-Ni Nanoparticles on Boron-Doped Diamond for Direct Ethanol Fuel Cell Applications

Christos K. Mavrokefalos[a], Maksudul Hasan*[a,b], James F. Rohan[b], John S. Foord*[a]

Abstract: In this work, electrochemical deposition of Pd (palladium) and bimetallic Pd-Ni (nickel) nanoparticles on oxygen-terminated boron-doped diamond (BDD) substrate is described for use as electrocatalyst in direct ethanol fuel cell. A potentiostatic two-step electrochemical method involving the electrodeposition of Ni nanoparticles on BDD followed by mono-dispersed Pd nanoparticles was used for the fabrication of Pd-Ni/BDD electrode. The electrocatalytic activity of the bimetallic Pd-Ni nanoparticles was evaluated in an alkaline solution containing ethanol and compared to that of the Pd nanoparticles alone. The bimetallic Pd-Ni nanoparticles showed 2.4 times higher mass activity than the similar systems from literature as well as stability when operated in alkaline media. Higher electrochemical response towards the electrooxidation of ethanol observed for the bimetallic electrocatalysts was due to the synergistic effects of the electron interaction at the interface of the two metals. Chronopotentiometric measurements revealed that Pd is more stable when anchored to the Ni nanoparticles. The optimised loading of mono-dispersed Pd on a foreign Ni metal as nanoparticles plays a crucial role in achieving a high mass (3.63×10^6 mA/g) and specific (10.53 mA/cm^2) electrocatalytic activity of Pd towards ethanol electrooxidation in alkaline media.

1. Introduction

Fuel cell are receiving increasing attention in recent years due to their ability to increase overall energy efficiency. The direct alcohol alkaline fuel cell (DAAFC) subcategory has attracted signficant research efforts because of the possibility to use non-noble materials, which are more stable in alkaline media and thus, reduce the noble metal content, the main cost component of the electrocatalysts. The DAAFC is able to convert the chemical energy stored in the fuel (i.e. alcohol) into electricity directly and therefore, can be used as the power source in portable electronics, transportation and other emerging applications.[1–4]

Hybrid materials, consisting of graphitic nanostructures (carbon nanotubes or graphene, for instance) and various metal particles have been widely studied as functional components in catalysis and fuel cell applications.[4–6] BDD is an alternative carbon substrate due to its unique features, such as wide potential window, low background capacitive current, chemical stability and robustness under hostile environments (potential, temperature, pressure), which have been described further in previous reports.[7–14] A number of recent review articles have presented the use of diamond electrodes for fundamental electrochemistry, bio-electrochemistry, photoelectrochemistry and related applications.[15-17] Diamond electrodes can be modified by metal nanoparticles enhancing its sensitivity towards various analytes compared to the unmodified electrode.[7,18-21] Of note is the resistance of diamond to electrocorrosion, a fact which make it attractive especially in the field of fuel cell.[22-24] Pt is one of the most effective electrocatalysts and used widely; nevertheless, the high cost as well as its tendency to be poisoned by the reaction intermediates during the ethanol electrooxidation can be prohibitive for future use.[25,26] Because of the aforementioned reason, core-shell structures[8,27-32] and the embodiment of non-noble metals[8,29,33] promise to enhance the stability of the electrocatalysts in DAAFC as well as to reduce their cost. One of the challenges in this field is also the development of efficient electrocatalysts capable to produce CO_2 after the ethanol electrooxidation or in other words to cleave the C-C bonds.[34] Pd has shown recently that can be more active, stable and poison tolerant towards the intermediates of ethanol electrooxidation species.[35-38] Furthermore, Pd is 50 times more earth abundant than its counterpart Pt and is a promising candidate to replace the latter in the field of alkaline fuel cell.[39]

In the present study, the modification of oxygen-terminated BDD electrodes with Pd and Pd-Ni nanoparticles is proposed for ethanol oxidation of relevance to the direct ethanol alkaline fuel cell (DEAFC). The motivation for this work is ultimately the continuation of our understanding of how metallic interfaces formed on the Ni nanoparticles agglomerate with partial coverage of mono-dispersed Pd nanoparticles behave on diamond by comparison with similar structures on other forms of carbon.[8] The second objective of this study is to gain a further understanding of how different core metals behave on diamond and how they can affect the stability, electrochemical activity and finally the poison tolerance towards the by-products of ethanol electrooxidation. In both of these cases, the electrochemical modifications introduced by the electrodeposition of the metal nanoparticles reflect the particular properties of the metal, the interface interaction between the two metals and their interaction with the underlying diamond.

2. Results and Discussion

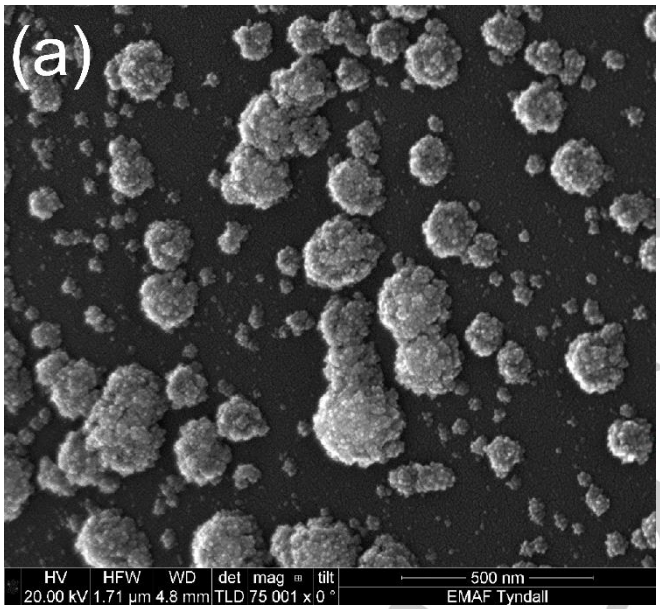
2.1 Morphology, EDX and XPS Characterisation of the Deposits on BDD Electrode

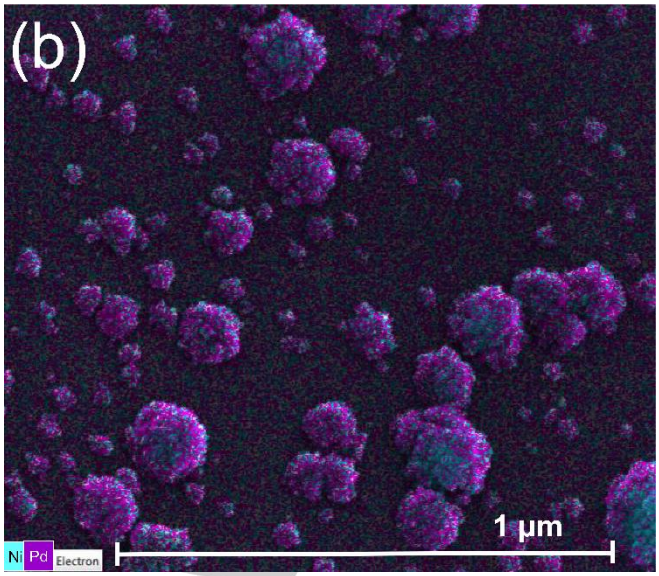
[a] Dr. C. K. Mavrokefalos, Dr. M. Hasan, Prof. J. S. Foord
Department of Chemistry, Chemistry Research Laboratory
University of Oxford
Mansfield Road, Oxford, OX1 3TA, England, UK
E-mail: maksudul.hasan@chem.ox.ac.uk, john.foord@chem.ox.ac.uk
[b] Dr. M. Hasan, Dr. J. F. Rohan
Tyndall National Institute
University College Cork
Lee Maltings, Cork, Ireland

Accepted Manuscript

This article is protected by copyright. All rights reserved.

The morphology of the deposits was characterised by a scanning electron microscope and the images are shown in Fig. 1 (a-b). Ni particles have been deposited in a non-uniform manner along the diamond edges with visible agglomeration as can be seen from the Figure 1(a) due to the high metal loading (658 mC/cm^2). The size of the Ni particles cannot be estimated due to the latter effect. The lateral conductivity of diamond as well as the non-uniform distribution of the B dopant led to the non-uniform distribution of the deposits as reported previously.[8] The sequential deposition of Pd onto Ni produced smaller particles around 13 nm as shown in elemental mapping of Figure 1(b). The elemental mapping provides information for the deposition of the Pd-Ni nanoparticles in which Pd nanoparticles quite sparsely cover the Ni particles. The elemental composition of the electrodes is displayed in Figure 1(c). Energy dispersive x-ray spectra shows slightly more intense Ni peaks than the Pd as expected from the low amount of Pd metal loading by comparison with Ni.





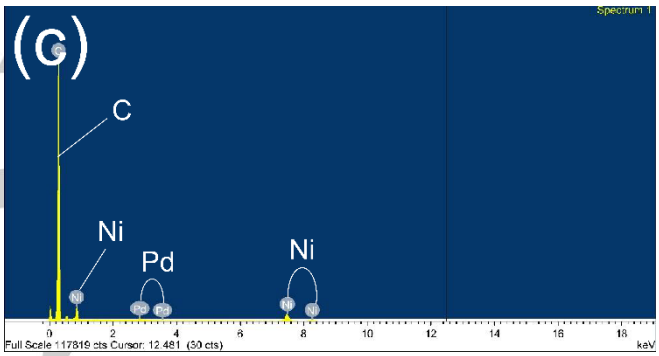


Figure 1. (a) SEM image of Ni deposited on BDD electrodes. (b) Elemental mapping of Pd-Ni deposited on BDD showing Ni nanoparticles agglomerate with partial coverage of mono-dispersed Pd nanoparticles. (c) EDX spectra of the Pd-Ni nanoparticles on BDD electrode.

The elemental composition as well as chemical and electronic states were explored by x-ray photoelectron spectroscopy as shown form the XPS spectra in Figure 2. Figure 2 (a) shows the wide scan survey of the oxygen-terminated BDD electrodes with the relevant elements of Ni, Pd and Pd-Ni. The wide scan survey illustrates the existence of C, O and the relevant peaks of the main metals. Figure 2 (b) illustrates the Ni 2p peaks of the Ni/BDD and Pd-Ni/BDD electrodes. The Ni modified BDD has Ni $2p_{3/2}$ and Ni $2p_{1/2}$ peaks at 856.6 eV and 874.5 eV, respectively.[40] The Ni photoelectron peak of the Pd-Ni/BDD electrode is attenuated significantly. As has been reported in previous work[8] the most likely scenario is that the Pd has covered the underlying Ni. The Pd modified BDD has two main peaks, the Pd $3d_{5/2}$ at 336.4 eV and Pd $3d_{3/2}$ at 341.7 eV, respectively. The Pd photoelectron peak of the bimetallic electrode has the same peaks. There is a binding energy shift of 0.2 eV, which implies an electronic interaction between the two metals. The negative shift of binding energy can be attributed to the increase in interfacial charge of Pd atoms relative to the bulk material, and charge transfer that occurred

Accepted Manuscript

This article is protected by copyright. All rights reserved.

from Ni atoms into the Pd contact layer, which increased the electron cloud densities of Pd atoms, as reported elsewhere.[41]

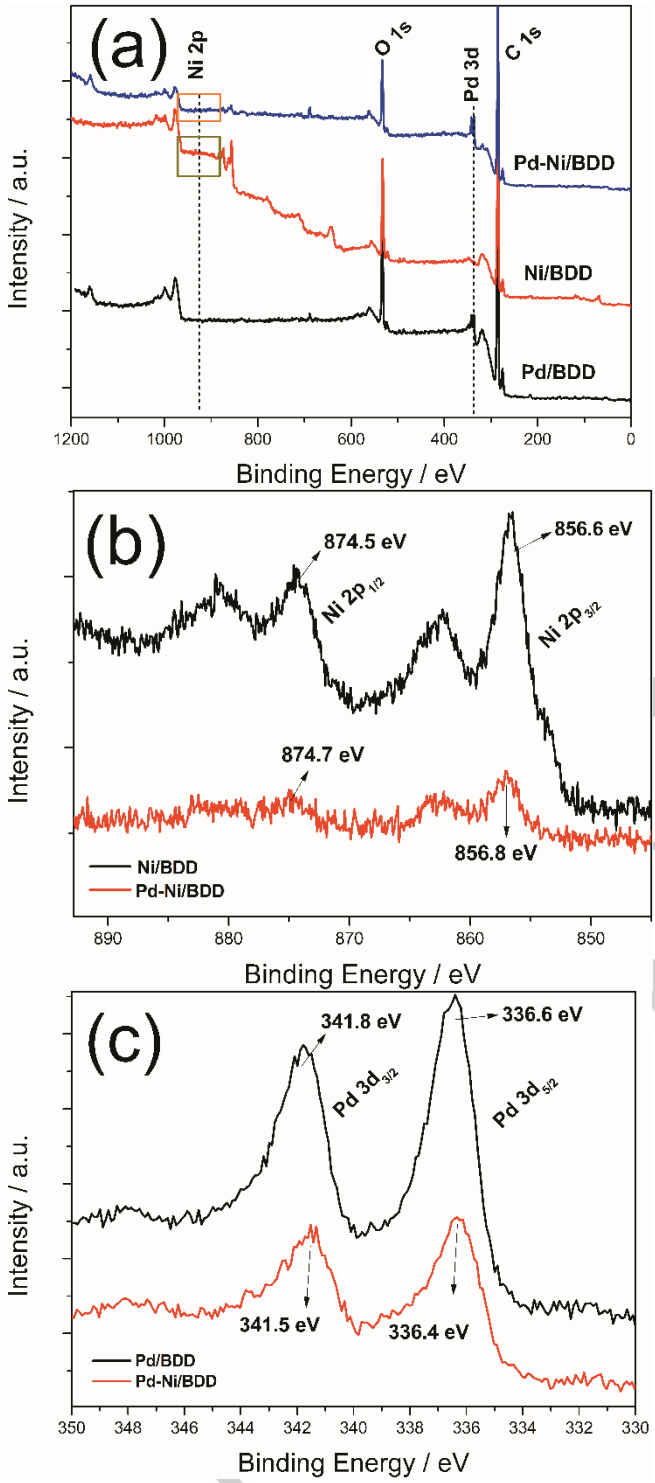
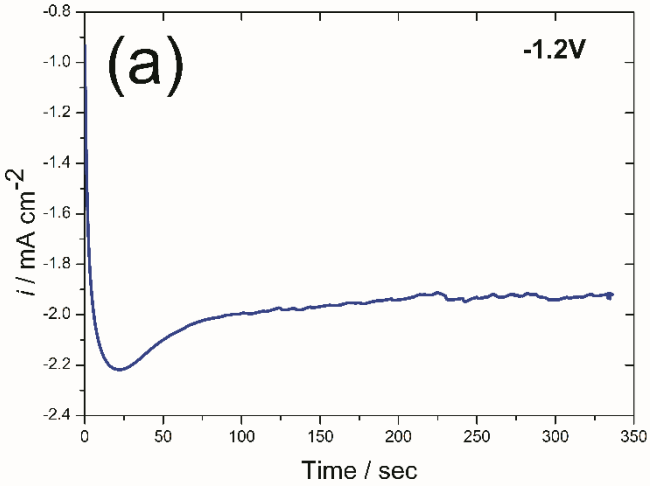


Figure 2. XPS spectra of (a) wide scans of the Ni/BDD, Pd/BDD and Pd-Ni/BDD, respectively, (b) typical Ni 2p peaks of the Ni and (c) typical Pd 3d peaks of the Pd in Pd-Ni modified BDD electrocatalysts.

2.2 Voltammetric Characterisation

2.2.1 Electrodeposition of the Electrocatalysts

A typical chronoamperogram of bare BDD in a solution containing 0.01 mol L^{-1} $[Ni(NO_3)_2 \cdot 6H_2O]$ in acetate buffer is shown in Figure 3(a). The Ni is deposited at a constant potential of -1.2V until 658 mC/cm^2 was passed. The increase in current for the first 25 seconds indicate the formation of small Ni nuclei followed by further growth of the nuclei, which decreases and finally becomes constant under the diffusion controlled reduction of the electroactive nickel ions. A typical cyclic voltammogram of the bare BDD in a solution containing 1mM $PdCl_2$/0.1 mol L^{-1} HCl is also illustrated in Figure 3(b). The deposition of Pd occurs in the potential range of +0.3V and -0.35V. In this region, there is a cathodic current peak maximum at +0.15V (peak C_1). This current remained stable until an overpotential value of -0.26V and then increased again sharply until reaching a maximum at -0.35V (peak C_3). The small cathodic peak C_2 (-0.15V) is due to the adsorption of the underpotentially deposited hydrogen (H_{UPD}) onto the Pd surface. The peak C_3 around -0.35V can be described as the diffusion limited reduction of Pd ions. After this point, there is a cathodic current at -0.37V (peak C_4) which represents the area of the simultaneous Pd deposition and bulk hydrogen evolution onto the freshly deposited Pd particles. Due to the latter process, peaks A_2, A_3 and A_4 correspond to the H desorption process. The A_1 peak shows the Pd stripping from the electrode surface having a maximum peak at +0.60V in the backward scan.



Accepted Manuscript

This article is protected by copyright. All rights reserved.

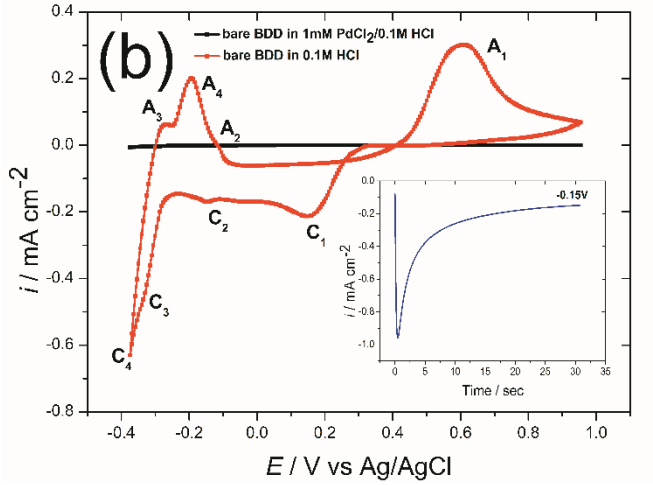


Figure 3. (a) Chronoamperogram of bare BDD in a solution containing 0.01 mol L^{-1} $[Ni(NO_3)_2{\cdot}6H_2O]$ in acetate buffer at constant potential of -1.2V. (b) Cyclic voltammogram of bare BDD in a solution containing 0.1 mol L^{-1} HCl and 1 mmol L^{-1} $PdCl_2$/0.1 mol L^{-1} HCl, respectively, at scan rate of 0.01 V s^{-1} (inset: chronoamperogram of Pd deposition from 1 mmol L^{-1} $PdCl_2$/0.1 mol L^{-1} HCl on bare BDD at constant potential of -0.15V).

2.2.2 Electrochemical Activity of the Electrocatalysts

All the electrocatalysts were electrochemically characterised by cyclic voltammetry and linear sweep voltammetry in 0.5M KOH as shown in Fig. 4. Fig. 4(a) shows the voltammograms of the bare BDD, Ni, Pd and Pd-Ni modified BDD with 2.9 μg/cm^2 Pd loading. There is no electrochemical activity on the unmodified electrode and the current response is close to zero. The Ni/BDD is not electrochemically active within the potential window in which Pd is active. Peaks A_2/C_2 represent the oxidation and reduction of freshly deposited Ni particles on the diamond surface at +0.49 and +0.43V, respectively.

Regarding the Pd/BDD electrode various features are observed: (i) Pd oxidation and reduction peaks (A_1/C_1) in the anodic scan at +0.05V and cathodic scan at-0.24V, respectively; these peaks can be attributed to the formation and removal of a palladium oxide layer on the surface of the electrocatalyst. The mechanism of the Pd oxidation formation was reported previously,[33,41,42] in which OH^- ions are chemisorbed in the initial stage of the oxide formation and then are transformed into higher valence oxides at higher potentials. (ii) Hydrogen adsorption and desorption peaks of Pd surface at -0.67V and -0.58V (C_3 and A_3).

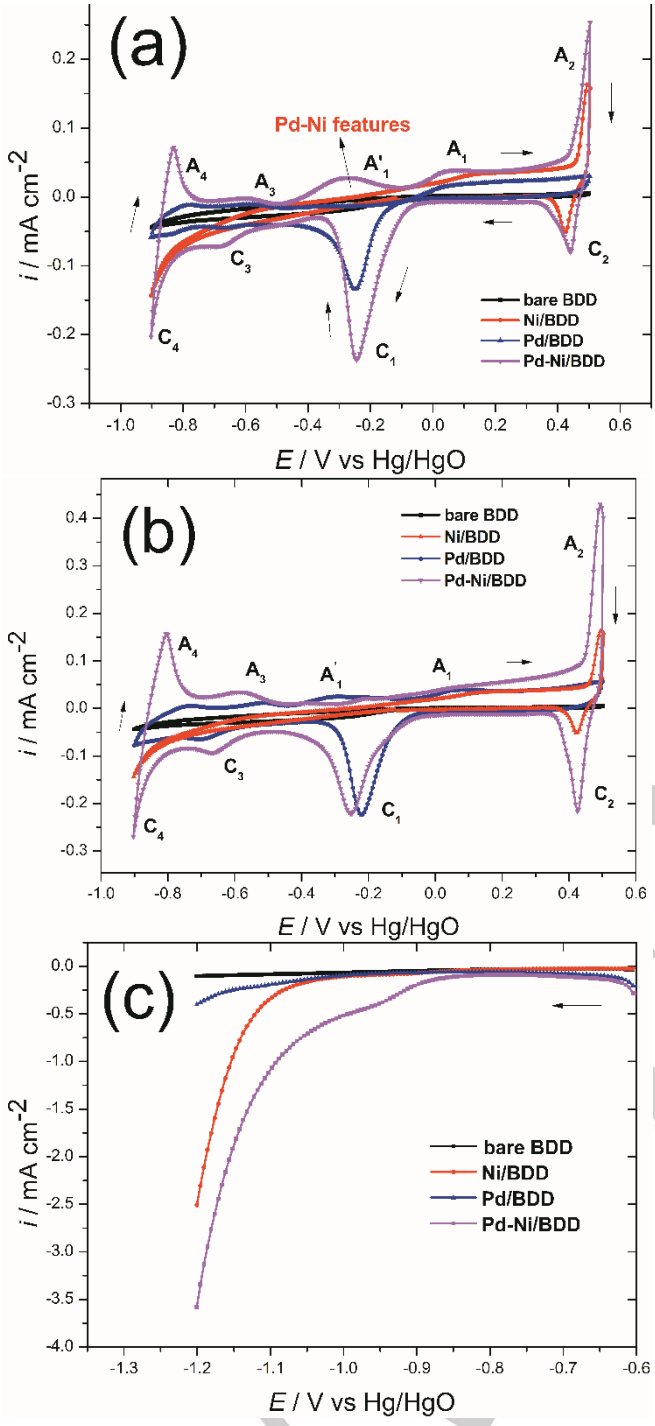
The Pd-Ni/BDD has the same features as the Pd/BDD but with higher electrocatalytic response. The features include (i) Pd oxidation and reduction waves occur at +0.05V (A_1) and -0.24V (C_1), respectively. (ii) H adsorption and desorption occurred on Pd surface between -0.67V in the cathodic scan (peak C_3) and -0.58V in the anodic scan (peak A_3), respectively. (iii) Ni oxidation and reduction waves appeared at +0.5V (A_2) and +0.44V (C_2), respectively and are consistent with the literature for the Ni-water system under ambient conditions[43], and (iv) a prepeak (A'_1) appeared at -0.27V in the anodic (backward) scan corresponds to oxidation at favourable sites on the palladium surface[44] and is not seen at its Ni and Pd counterparts. The latter feature may be consistent with the Ni particles serving as reactive centres for the subsequent deposition of Pd as a result the metallic interfaces between Ni and Pd nanoparticles.

The mechanism for the formation of core-shell nanoparticles has been discussed in our previous work with Pt and Cu nanoparticles on oxidised diamond electrodes.[8] A pronounced hydrogen adsorption and evolution occurred on the Pd-Ni surface in the cathodic scan at -0.9V (peak C_4) and the corresponding desorption occurred in the anodic scan at -0.87V (peak A_4). Figure 4(b) shows the cyclic voltammograms of the same electrodes but with 4 times more Pd loading (11.6 μg/cm^2). We can observe similar features but with a little higher current response due to the higher amount of Pd loading on Ni surface. However, in the case of the higher amount of Pd loaded bimetallic electrocatalyst the characteristic oxidation prepeak (A'_1) was not seen. This likely arises due to the fact that 4 times more Pd has created a thick layer on top of the Ni particles and therefore, is unable to have the electronic interaction between the two metals and negates the advantages of core-shell structure. Figures 4 (c and d) illustrate the linear sweep voltammograms of the above electrocatalysts with 2.9 μgr/cm^2 and 11.6 μgr/cm^2 Pd loading on Ni particles, respectively. All the electrocatalysts were scanned into the hydrogen evolution region starting from -0.6V and ending at -1.2V. In both cases, there is no electrocatalytic response for the unmodified BDD. The Pd/BDD electrodes showed lower current response and therefore, lower hydrogen evolution than the Ni/BDD. The maximum current densities were provided by the bimetallic core-shell electrocatalysts giving the highest hydrogen adsorption and evolution on their surface.

The metal coverage of Pd can be estimated from the charge of the Pd oxide reduction peak C_1 in Fig. 4(a-b). The ratio of the charge required for desorption of an oxygen monolayer on the Pd (111) surface[45] (0.424 mC/cm^2) to that of Q_{des}, which is the coulombic charge of the oxygen desorption on the Pd surface, determines the electroactive surface area (EAS) of the pure Pd electrocatalyst. In addition, the specific surface area (SSA) can be defined as the electroactive surface area divided by the metal loading. All the above information is included in the Table 1. The electroactive as well as the specific surface areas are doubled in the case of the Pd-Ni/BDD electrocatalysts.

Accepted Manuscript

This article is protected by copyright. All rights reserved.



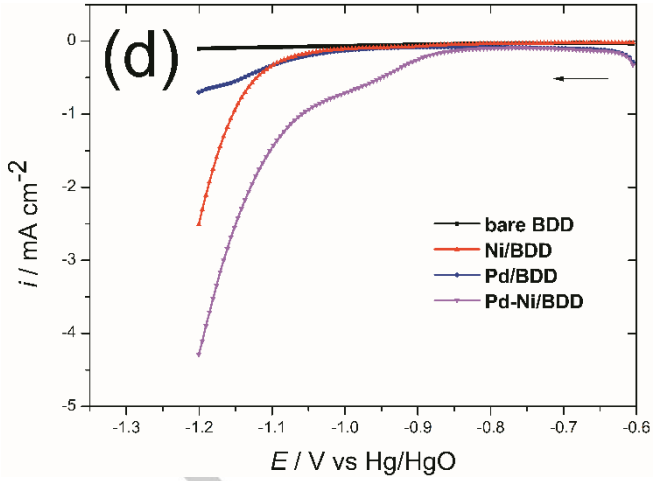


Figure 4. Cyclic voltammograms (a and b) and linear sweep voltammograms (c and d) of the Ni/BDD, Pd/BDD (Pd loading: 2.9 (a) and 11.6 (b) μg/cm^2) and Pd-Ni modified BDD (Pd loading: 2.9 (a) and 11.6 (b) μg/cm^2) in 0.5 mol L^{-1} KOH solution at scan rate of 0.02 V s^{-1} (all CVs and LSVs were started from open circuit potential). The amount of Ni loading were the same for all electrodes (658 mC/cm^2).

2.3 Evaluation of Pd-Ni Electrocatalysts Preparation Conditions on Ethanol Oxidation Characteristics

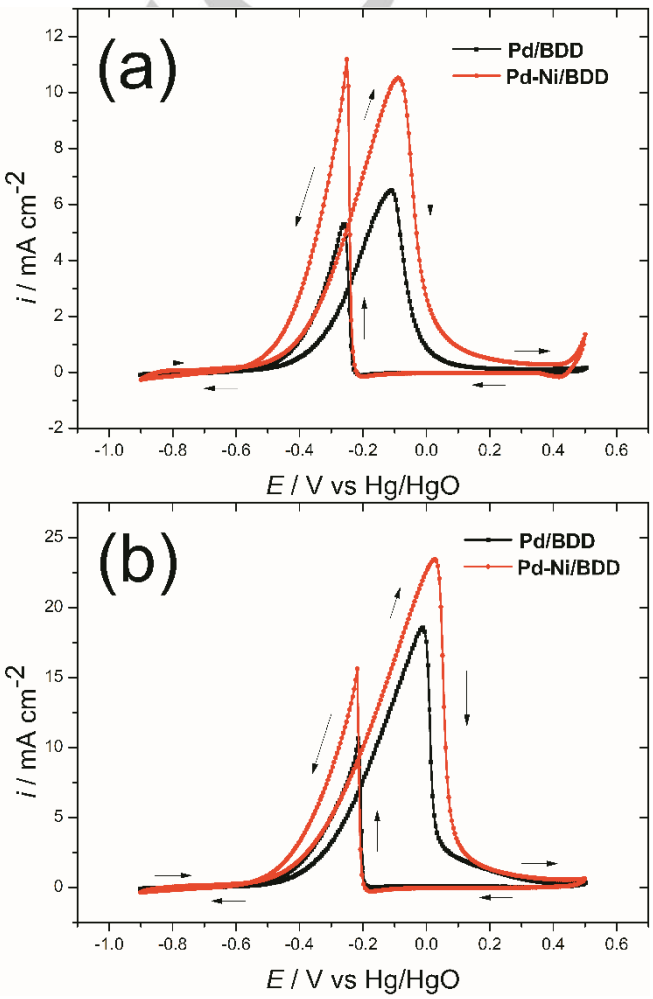
The Pd-Ni/BDD electrocatalysts were evaluated through cyclic voltammetry and compared to Pd/BDD alone towards the ethanol electrooxidation. Cyclic voltammograms of the modified electrodes were obtained after a scan in a solution containing 0.5M KOH and 1M EtOH and the results are shown in Figure 5(a) and (b). The onset overpotential is observed at -0.55V and all the electrodes are inactive before this overpotential. When the applied potential is scanned positively in the anodic scan an electrooxidation current is observed. The peak current due to the electrooxidation of ethanol on the electrodes appeared at around -0.08V, -0.1V, -0.01V and +0.03V for the Pd/BDD (2.9 μg/cm^2), Pd-Ni/BDD (2.9 μg/cm^2), Pd/BDD (11.6 μg/cm^2), and Pd-Ni/BDD (11.6 μg/cm^2), respectively, as shown in Figure 5 (a) and (b). It appears that the corresponding peak potentials move in the cathodic direction with Ni anchoring and in the anodic direction with increasing Pd loading. The synergy of the electron interaction between the outermost d-orbitals of the Ni and Pd metals as discussed in section 3.1 increases the electron cloud at the interfacial layer and thus, facilitates faster adsorption of the hydroxyl and ethanol species towards electrooxidation. Conversely, higher loading of Pd onto Ni increases the thickness of the interfacial layer and thus, minimises the synergistic effects of the electron interaction. The current density in the forward peak (I_f) of ethanol electrooxidation of Pd-Ni/BDD (2.9 μg/cm^2) was acquired at 10.5 mA/cm^2 while the same peak of the Pd/BDD (2.9 μg/cm^2) was obtained at 6.5 mA/cm^2. The peak in the anodic scan is due to the electrooxidation of the fresh carbonaceous species of ethanol accumulated on the surface of the electrode. After this oxidation wave, all the electrodes deactivated at around 0.1V (Pd/BDD) and 0.2V (Pd-Ni/BDD) for the electrodes in Figure 5(a) and at around 0.4V for the electrodes in Figure 5(b). The

Accepted Manuscript

This article is protected by copyright. All rights reserved.

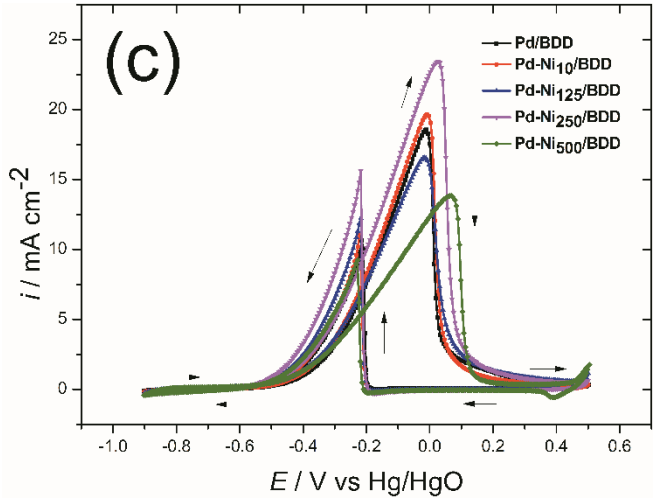
electrodes with 2.9 μg/cm^2 Pd loading are activated again at -0.22V (Figure 5a) and the electrodes with 11.6 μg/cm^2 Pd loading at -0.19V giving a second electrooxidation peak (I_b) at -0.25V (Pd: 2.9 μg/cm^2, Figure 5a) and at -0.21V (Pd: 11.6 μg/cm^2, Figure 5b), and these peaks are due to the oxidation of the incompletely oxidised carbonaceous species of ethanol that are still on the surface of the electrode after the anodic scan. The corresponding current density with higher Pd loaded bimetallic electrode (11.6 μg/cm^2) were found to be 23.4 mA/cm^2 whereas the current density peak with the equivalent amount of Pd alone was 18.5 mA/cm^2. It is interesting to point out that Pd loading was increased by 4 times in Figure 5(b) by comparison with that in Figure 5(a) but the current density increased only by about 2.2 times, which implies that higher amount of Pd onto Ni metal disaffirm the synergistic effects of the interfaces on the nanostructured metallic surfaces. However, in the context of the poisoning tolerance i.e., ratio of the peak forward current (I_f) to back (I_b), the higher amount of Pd on Ni metal particle is more tolerant towards the ethanol electrooxidation. The values of the poison tolerance ratios are presented in Table 1. The mass activity of the Pd-Ni (Pd loading: 2.9 μg/cm^2) electrocatalysts towards ethanol electrooxidation has been compared with the most recent studies in literature and found that our electrocatalysts showed 2.4 times higher mass activity compared to similar system.[46] Moreover, our monometallic Pd/BDD (Pd loading: 2.9 μg/cm2) electrocatalyst showed 8 times higher mass activity than its counterpart on a carbon support (Pd/C).[46,47]

Figure 5(c) illustrates electrooxidation of ethanol on Pd-Ni/BDD electrode with 11.6 μg/cm^2 Pd loading versus different amount of Ni loading. The purpose of that investigation was to find out the optimum amount of Ni needed to interact electronically with the outer Pd shell. Hence, we observe that a very small amount of Ni behaves the same as the pure Pd/BDD electrocatalyst offering negligible synergistic effects of the electron interaction at the interface of the Pd and Ni metal. Conversely, an electrode with up to 25 times higher deposition charge of Ni_{250} (200 μg/cm^2) is needed in order to realise such synergistic effects of the electron interaction at the interfaces between two metals. The current density decreased again with a further increase in deposition charge of Ni as seen for Pd-Ni_{500}/BDD electrode. Clearly, it is very important that the optimum shell-core metal ratio is achieved not only for the particular properties of the metal but also of the synergistic effects of the interfaces between two metals. It is widely accepted that chemisorbed CO species has been identified as a predominant poisoning species for the ethanol oxidation reaction on the electroactive sites of the catalyst.[48] According to a recent study, a proposed mechanism for the CO chemisorption reaction is the following[49]: $CO_{ads} + OH_{ads} \rightarrow CO_2 + H_2O$, where CO_{ads} and OH_{ads} represent the radicals adsorbed on the electroactive sites. Hence, an adequate shell-core metal ratio for an optimised and effective metallic interface can increase the poisoning tolerance towards the electrooxidation of alcohol as can be seen from the increased ratio of peak forward current (I_f) to back (I_b) in Figure 5(b) and works as protection for the noble metal typically poisoned by the carbonaceous intermediates of the alcohol. The optimum Pd loading in terms utilisation efficiency coupled with increased tolerance towards the carbonaceous intermediate species produced during ethanol electrooxidation was 2.9 μg/cm^2 on Ni_{250}/BDD electrode. However, of note is the fact that the mass activity of the ethanol electrooxidation on Pd-Ni electrocatalyst with 4 times less Pd loading is 2.25 times higher than that of the Pd alone. All the aforementioned results have been summarised in Table 1. Stability tests were conducted in alkaline solution. There was only a 12% decrease of the current density on the Pd-Ni electrocatalyst instead of 35% current drop on the Pd alone. The proposed mechanism for Ni atoms donating electron cloud to the Pd interfacial contact layer that facilitates the faster electrooxidation of ethanol species is illustrated in Figure 5(d).



Accepted Manuscript

This article is protected by copyright. All rights reserved.



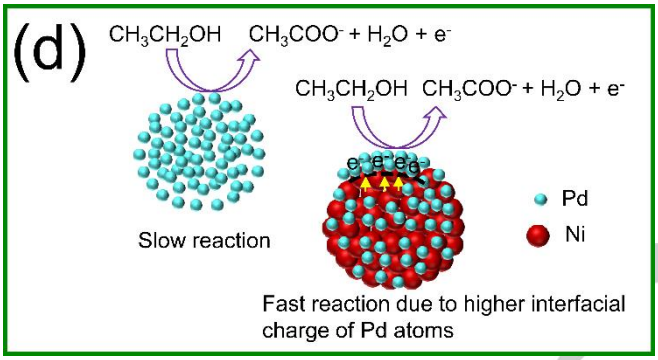


Figure 5. (a, b) Cyclic voltammograms of Pd and Pd-Ni modified BDD with 2.9 μg/cm^2 (i.e., 5.2 mC/cm^2 charge) and 11.6 μg/cm^2 (i.e., 21 mC/cm^2 charge) Pd loading, respectively in 0.5 mol L^{-1} KOH and 1 mol L^{-1} EtOH at scan rate of 0.1 V s^{-1}. The amount of Ni loading in Figure 5(a) and 5(b) was Ni_{250} (200 μg/cm^2). (c) Cyclic voltammograms of Pd and Pd-Ni modified BDD (with 2.9 μg/cm^2: Pd loading versus different amount of Ni loading) in 0.5 mol L^{-1} KOH and 1 mol L^{-1} EtOH at scan rate of 0.1 V s^{-1}. (all CVs were started from open circuit potential). The subscript value in the legend in (c) represents the deposition charge of Ni in mC/cm^2 with corresponding equivalent weight for Ni_{10}, Ni_{125}, Ni_{250} and Ni_{500} to 8 μg/cm^2, 100 μg/cm^2, 200 μg/cm^2 and 400 μg/cm^2, respectively. Cyclic voltammograms shown here are steady-state taken after 10 cycles. (d) Schematic of Pd-Ni atomic arrangement with Ni atoms donating electron cloud to the Pd interfacial contact layer thus facilitating the faster electrooxidation of ethanol species.

2.4 Tafel Analysis

Further investigation of the electrocatalytic activity of the electrocatalysts performed through Tafel analysis. The measurements recorded the anodic polarisation curve during the electrooxidation of ethanol and analysed the kinetic parameters. Quasi-steady-state cyclic voltammograms were used to make the Tafel plots and the results are demonstrated in Figure 6. The lower onset potential region of -0.6V to -0.25V, known as the charge transfer control region, is dominated by the adsorption of hydroxyl ions on the Pd surface as reported in previously.[41,42] In Figure 6(a), slopes in the lower onset potential are 184.2 mV dec^{-1} and 201.8 mV dec^{-1} for the Pd/BDD and Pd-Ni/BDD, respectively, with the lower amount of Pd loading (2.9 μg/cm^2). The Tafel slope indicates the kinetics of ethanol oxidation in the above potential region and is controlled by the adsorption of hydroxyl ions. A small deviation in the Tafel slope between the Pd/BDD and Pd-Ni/BDD indicates that the kinetics of the electrooxidation of ethanol is controlled by the additional surface reactions such as the formation of oxide layer as we reported in our previous study.[41] A similar description can be applied to the higher Pd loaded electrode (11.6 μg/cm^2) in Figure 6(b). All the plots have been fitted to a linear region. In Figure 6(b), the slope of the Pd/BDD is 178 mV dec^{-1} a bit lower than that of Pd-Ni/BDD (203.2 mV dec^{-1}). This is likely due to the adsorption of more hydroxyl (OH_{ads}) ions on the surface of the Pd-Ni nanoparticles with higher palladium loading. The Tafel slopes are similar for all electrodes and good agreement with the Temkin type adsorption for hydroxyl (OH_{ads}) and acyl (CH_3CO_{ads}) ions in the lower onset potential region (-0.6V to -0.25V) indicating the similarity of the reaction mechanism for ethanol electrooxidation.[44]

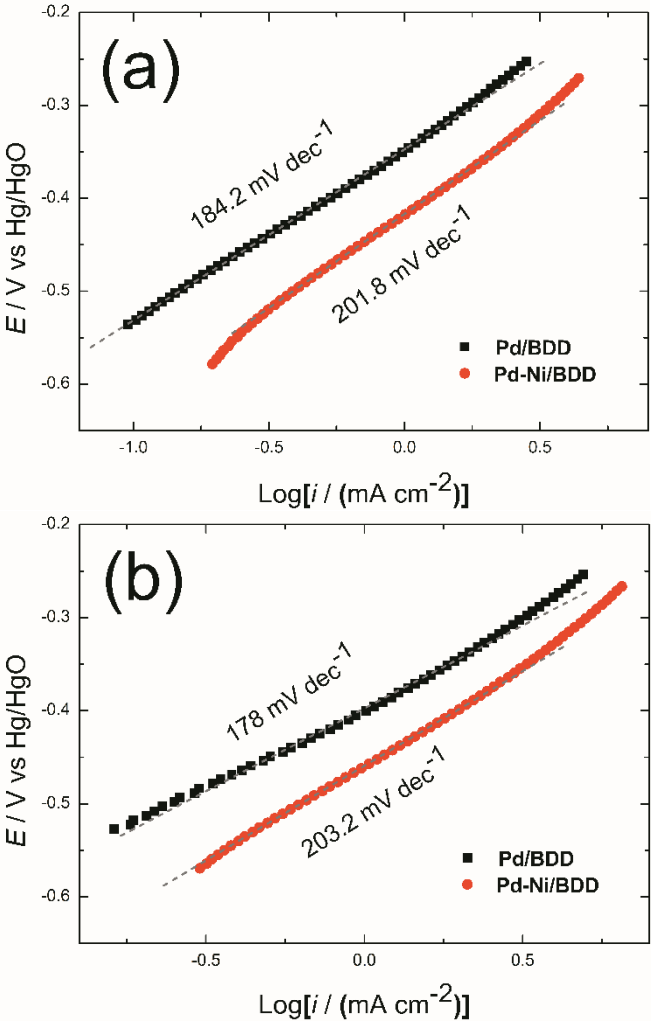


Figure 6. Tafel plots of anodic polarisation curve for ethanol electrooxidation in 0.5 mol L^{-1} KOH and 1 mol L^{-1} EtOH: Pd/BDD and Pd-Ni/BDD electrode with Pd

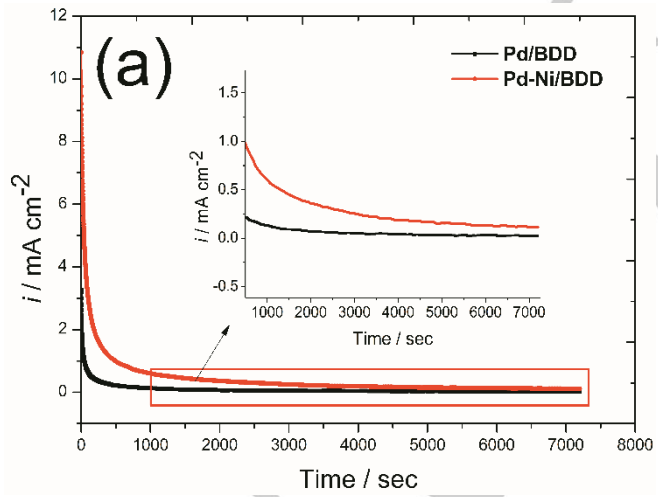
Accepted Manuscript

This article is protected by copyright. All rights reserved.

loading of (a) 2.9 μg/cm^2 (i.e., 5.2 mC/cm^2) and (b) 11.6 μg/cm^2 (i.e., 21 mC/cm^2), respectively. The amount of Ni loading was Ni_{250} (200 μg/cm^2).

2.5 Amperometric Response of the Electrocatalysts in Ethanol

In order to compare the stability of Pd-Ni electrocatalysts with the Pd only on BDD version chronoamperometric experiments were carried out towards the electrooxidation of ethanol and the results are seen in Figure 7. All the electrodes were held at a fixed and constant potential of -0.15V and run for 2 hours. The current densities decreased initially for all electrodes and stabilised at 2 hours operational time in the range of 0.2-0.4 mA/cm^2 (Figure 7a), which is ascribed to the combined effects of electrocatalyst poisoning by the chemisorbed carbonaceous oxidative intermediates and the concentration polarisation with time (i.e., limited mass transport with increasing reaction time). However, the core-shell electrocatalysts showed a higher current response in relation to the Pd alone. Of note is that the Pd-Ni/BDD with only 2.9 μg/cm^2 Pd loading gave a higher amperometric response than the pure Pd/BDD with almost 4 times higher palladium loading (11.6 μg/cm^2) (Figure 7b). The latter can be attributed to the fast electrocatalyst poisoning by some of the carbonaceous intermediates of the ethanol oxidation reaction in the absence of Ni metal. In contrast, the activity of the Pd supported on Ni nanoparticles was enhanced and through the electronic interaction effects of the Ni/BDD support protected the electrocatalyst for a longer period.



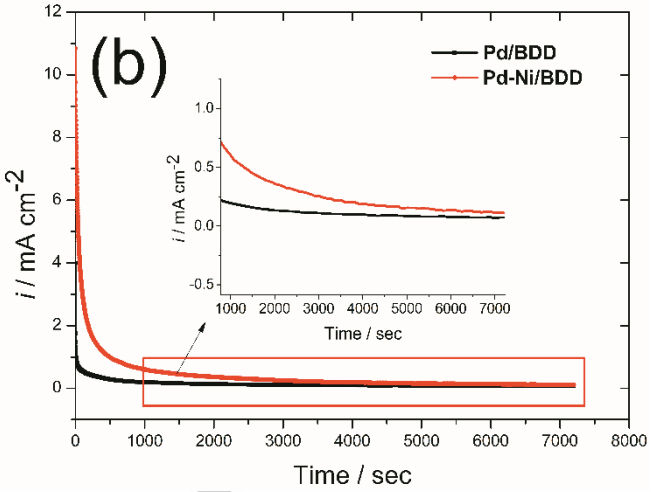


Figure 7. (a) Chronoamperometric response of Pd and Pd-Ni modified BDD with Pd loading of (a) 2.9 μg/cm^2 (i.e., 5.2 mC/cm^2) and (b) 11.6 μg/cm^2 (i.e., 21 mC/cm^2), respectively, in 0.5 mol L^{-1} KOH and 1 mol L^{-1} EtOH at potential -0.15V. The Ni loading was Ni250 (200 μg/cm^2).

Accepted Manuscript

This article is protected by copyright. All rights reserved.

Table 1. Pd features after electrodeposition through chronoamperometry on Ni_{250}/BDD.

Electrodes	Charge (mC cm^{-2})	Pd loading (µg cm^{-2})	Qdes charge (mC cm^{-2})	Electroactive surface area, EAS (cm^2 cm^{-2})	Specific surface area, SSA (m^2 g^{-1})	Mass activity (mA g^{-1}) x 10^6	Forward peak current (I_f), specific activity (mA cm^{-2})	Poisoning tolerance I_f/I_b
Pd/BDD	5.2	2.9	0.24	0.56	19.31	2.25	6.52	1.23
Pd-Ni/BDD			0.46	1.08	37.24	3.63	10.53	0.94
Pd/BDD	21	11.6	0.27	0.63	5.43	1.60	18.56	1.75
Pd-Ni/BDD			0.48	1.13	9.74	2.02	23.47	1.50

3. Conclusions

The enhanced mass activity and stability of Pd-Ni bimetallic nanoparticles supported on BDD electrodes were shown in this work. The BDD surface was modified electrochemically with the electrodeposited metal nanoparticles. A two-step electrochemical deposition method was used for the fabrication of the Pd-Ni nanoparticles onto the BDD surface. A potentiostatic method was used to deposit noble metal Pd and transition metal Ni as nanoparticles onto BDD to investigate their electrocatalytic properties for ethanol electrooxidation and its electrocatalytic activity by comparison with that of Pd alone. Electrochemical characterisation and XPS suggested that Ni particles serve as reactive centres for the subsequent deposition of mono-dispersed Pd nanoparticles with partial coverage in order to form interfaces between the two metals. The latter modification led to higher ethanol oxidation current densities than for Pd/BDD alone owing to the synergistic effects of electron interaction at the metallic interfaces. Our synthesised Pd-Ni/BDD electrocatalyst showed 2.4 times higher mass activity than similar systems from literature as well as the stability when operated in alkaline media. Furthermore, electrochemical experiments revealed that the proper Pd loading tuning, in other words, thickness of the metallic interfaces, plays an important role in achieving high mass and specific electrocatalytic activity towards the ethanol electrooxidation. Finally, after chronoamperometric experiments, bimetallic Pd-Ni/BDD electrocatalysts showed a higher stability during the ethanol oxidation by comparison with Pd/BDD alone.

Experimental Section

Chemical Reagents

Chemical reagents were purchased from Sigma-Aldrich and used as received without any further purification. These were: palladium (II) chloride ($PdCl_2$); hydrochloric acid (HCl); nickel (II) nitrate hexahydrate [$Ni(NO_3)_2{\cdot}6H_2O$]; acetic acid and sodium acetate. All aqueous solutions were freshly prepared, using milli-Q water (>18 MΩ cm) and solutions were deaerated using oxygen-free nitrogen gas for a minimum of 20 minutes prior to running experiments.

Equipment and experimental Set-up

BDD wafers ([B]>10^{20} cm^{-3}) of 10 x 10 x 0.6 mm were obtained from Element Six Co. (UK) and mounted in a home-built PTFE holder with a circular area of 0.38 cm^2 exposed to the electrolyte. The electrochemical measurements were performed with an Autolab PGSTAT 128N potentiostat/galvanostat. The electrochemical depositions were conducted at room temperature (24 ± 1.0°C) using a standard three electrode cell with a Pt counter electrode and a Ag/AgCl (1M KCl) reference electrode. The electrochemical measurements of ethanol electrooxidation were carried out at room temperature using a three electrode cell with a Pt and Hg/HgO (1 mol L^{-1} KOH) as the counter and reference electrode, respectively. The data were analysed with OriginPro 8.5 software (OriginLab Ltd.). The morphology of the deposits was characterised by a high resolution FEI Helios Nanolab 600i field emission scanning electron microscope with an attached Oxford Instruments AZtech X-Max-80 energy dispersive X-ray spectroscopy unit for elemental mapping. All the images were taken at 400K magnification with an acceleration voltage of 20 kV and a working distance (WD) of around 4 mm. The composition of the deposits was measured by XPS using an Al Kα (1486.6 eV) X-ray source. XPS data were curve fitted using CasaXPS software,[50] using a Shirley background.[51] The C 1s peak was calibrated to 285 eV with the following relative sensitivity factors (R.S.F.): C 1s (1.0), O 1s (2.93), Pd 3d (16.0) and Ni 2p (22.2).

Modification of BDD electrodes

Prior to each use, to ensure fresh, active surfaces, free of deactivating layers and contamination, which consequently leads to better signal to noise in the electrochemical data.[52] BDD working electrodes were polished with alumina micropolish II (Buehler, UK) of decreasing particle size (1 µm to 0.05 µm) on soft lapping pads (Buehler, Chemonet I for 8'' wheel). When the polishing had been finished with the 1 µm alumina, the electrodes were rinsed gently with distilled water and were sonicated for 5 minutes in water and acetone (1:1 ratio). This was followed by polishing with 0.05 µm alumina, a rinse in water, and sonication for 30 minutes. The electrodes then were cycled in 0.1 mol L^{-1} nitric acid between the potential range of -1.7V and 2.5V for 10 sweeps, which yields a high concentration of oxygen functionalities at the electrode surface.[11]

Accepted Manuscript

This article is protected by copyright. All rights reserved.

Pd was then electrodeposited onto BDD from a deaerated 0.1 mol L^{-1} HCl solution containing 1 mmol L^{-1} $PdCl_2$ by a potentiostatic method. The deposition potential was held at -0.15V (vs Ag/AgCl) until 5.2 and 21 mC/cm^2 charge passed through the surface. The corresponding metal loading of the aforementioned charges was 2.9 and 11.6 µg/cm^2, respectively. The electrodepositions potential was chosen after cyclic voltammetry on bare diamond electrode in the aforementioned solution, a potential range (-0.1V to -0.4V) in which Pd reduction is occurred.[41]

The second electrode comprised Pd-Ni/BDD was fabricated as follows: Ni was electrodeposited onto BDD from a deaerated 0.01 mol L^{-1} $[Ni(NO_3)_2.6H_2O]$ in acetate buffer solution by a potentiostatic method. The deposition potential was held at -1.2V (vs Ag/AgCl) until 658 mC/cm^2 charge was passed through the surface. The Ni/BDD electrode then was removed, rinsed with ultrapure water and dried with N_2. Pd was then electrodeposited onto Ni/BDD from a deaerated 0.1 mol L^{-1} HCl solution containing 1 mmol L^{-1} $PdCl^2$. Again, a potentiostatic method was used in which the potential was held at -0.15V (vs Ag/AgCl) until 5.2 and 21 mC/cm^2 charge passed through the electrode surface giving 2.9 and 11.6 µg/cm^2 palladium loading as referred in the previous paragraph.

Acknowledgements

Authors acknowledge Marie Curie Actions co-funded Irish Research Council Elevate fellowship ELEVATEPD/2014/15.

Notes

The authors declare no competing financial interest.

Keywords: Diamond • Electrocatalyst • Bimetallic • Nanoparticles • Fuel Cell • Ethanol • Palladium • Nickel

[1] E. Antolini, *J. Power Sources* **2007**, *170*, 1–12.
[2] C. Bianchini, P. K. Shen, *Chem. Rev.* **2009**, *109*, 4183–4206.
[3] C. Lamy, A. Lima, V. LeRhun, F. Delime, C. Coutanceau, J. M. Léger, *J. Power Sources* **2002**, *105*, 283–296.
[4] A. Verma, S. Basu, *J. Power Sources* **2005**, *145*, 282–285.
[5] G. Pang, M. Sun, P. Liu, L. Hou, F. Gao, *RSC Adv*. **2016**, *6*, 19734–19741.
[6] Y. Li, L. Han, B. An B, Y. Wang, L. Wang, X. Yin, J. Lu, *J. Mater. Sci. Mater. Electron*. **2016**, *27*, 6208-6215.
[7] A. Kraft, *Int. J. Electrochem. Sci.* **2007**, *2*, 355–385.
[8] C. K. Mavrokefalos, G. W. Nelson, C. G. Poll, R. G. Compton, J. S. Foord, *Phys. Status Solidi Appl. Mater. Sci*. **2015**, *212*, 2559-2567.
[9] R. L. McCreery, *Chem. Rev*. **2008**, *108*, 2646–87.
[10] T. N. Rao, A. Fujishima, *Diam. Relat. Mater*. **2000**, *9*, 384–389.
[11] I. Shpilevaya, W. Smirnov, S. Hirsz, N. Yang, C. E. Nebel, J. S. Foord, *RSC Adv*. **2014**, *4*, 531-537.
[12] G. M. Swain, Thin-Film Diamond II. *Elsevier*, San Diego, **2017**.
[13] K. E. Toghill, L. Xiao, M. A. Phillips, R. G. Compton, *Sensors Actuators, B Chem*. **2010**, *147*, 642–652.
[14] K. E. Toghill, L. Xiao, N. R. Stradiotto, R. G. Compton, *Electroanalysis* **2010**, *22*, 491–500.
[15] J. V. Macpherson, *Phys. Chem. Chem. Phys.* **2015**, 17, 2935-2949.
[16] N. Yang, J. S. Foord, X. Jiang, *Carbon* **2016**, 99, 90-110.
[17] D. Luo, K. Nakata, A. Fujishima, S. Liu, *J. Photochem. and Photobio. C: Photochem. Reviews* **2017**, 31, 139-152.
[18] T. A. Ivandini, R. Sato, Y. Makide, A. Fujishima, Y. Einaga, *Anal. Chem.* **2006**, *78*, 6291–6298.
[19] D. K. Belghiti, M. Zadeh-Habchi, E. Scorsone, P. Bergonzo, *Procedia Eng.* **2016**, 168, 428-431.
[20] I. Sadok, K. Tyszczuk-Rotko, A. Nosal-Wiercinska, *Sensors Actutors B Chem.* **2016**, 235, 263-272.
[21] C. F. Pereira, A. B. Couto, M. R. Baldan, N. G. Ferreira, *ECS Transactions* **2015**, 64, 15-22.
[22] B. C. Ramos, E. Saito, V. J. Trava-Airoldi, A. O. Lobo , F. R. Marciano, *Surf. Coatings Technol*. **2014**, *259*, 732–736.
[23] C. A. G. S. Oliveira, M. F. Stein, E. Saito, H. Zanin, L. S. Vieira, L. Raniero, V. J. Trava-Airoldi, A. O. Lobo, F. R. Marciano, *Diam. Relat. Mater*. **2015**, *53*, 40–44.
[24] R. G. Compton, J. S. Foord, F. Marken, *Electroanalysis* **2003**, *15*, 1349–1363.2
[25] F. C. Nart, T. Iwasita, *J. Electroanal. Chem.* **1991**, *308*, 277–293.
[26] C. Qiu, R. Shang, Y. Xie, Y. Bu, C. Li, H. Ma, *Mater. Chem. Phys*. **2010**, *120*, 323–330.
[27] X. Ge, L. Chen, J. Kang, T. Fujita, A. Hirata, W. Zhang, J. Jiang, M. Chen, *Adv. Funct. Mater*. **2013**, *23*, 4156–4162.
[28] C. Hsu, C. Huang, Y. Hao, F. Liu, *Phys. Chem. Chem. Phys*. **2012**, *14*, 14696–701.
[29] J. Hu, X. Lu, J. S. Foord, *Electrochem. commun*. **2010**, *12*, 676–679.
[30] N. Kristian, Y. Yu, J. M. Lee, X. Liu, X. Wang, *Electrochim. Acta* **2010**, *56*, 1000–1007.
[31] Z. D. Wei, Y. C. Feng, L. Li, M. J. Liao, Y. Fu, C. X. Sun, Z. G. Shao, P. K. Shen, *J. Power Sources* **2008**, *180*, 84–91.
[32] C. J. Zhong, J. Luo, B. Fang, *Nanotechnology* **2010**, *21*, 062001.
[33] M. Hasan, S. B. Newcomb, J. F. Rohan, K. M. Razeeb, *J. Power Sources*. **2012**, *218*, 148–156.
[34] E. H. Yu, U. Krewer, K. Scott, *Energies* **2010**, *3,* 1499–1528.
[35] C. Xu, H. Wang, P. K. Shen, S. P. Jiang. *Adv. Mater*. **2007**, *19*, 4256–4259.
[36] F. Hu, C. Chen, Z. Wang, G. Wei, P. K. Shen, *Electrochim. Acta* **2006**, *52*, 1087–1091.
[37] H. T. Zheng, Y. Li, S. Chen, P. K. Shen, *J. Power Sources* **2006**, *163*, 371–375.
[38] C. Xu, P. Shen, Y. Liu, *J. Power Sources* **2007**, *164*, 527–531.
[39] E. Antolini, E. R. Gonzalez, *J. Power Sources* **2010**, *195*, 3431–3450.
[40] C. D. Wagner, W. M. Riggs, L. E. Davis, J. F. Moulder, G. E. Muilenburg, Handbook of X-Ray Photoelectron Spectroscopy, Perkin-Elmer Co, Minnesota, **1979**.
[41] C. K. Mavrokefalos, M. Hasan, W. Khunsin, M. Schmidt, S. A. Maier, J. F. Rohan, R. G. Compton, J. S. Foord, *Electrochim. Acta* **2017**, *243*, 310-319.
[42] Z. X. Liang, T. S. Zhao, J. B. Xu, L. D. Zhu, *Electrochim Acta* **2009**, *54*, 2203–2208.
[43] F. Ciesielczyk, P. Bartczak, K. Wieszczycka, K. Siwinska-Stefanska, M. Nowacka, T. Jesionowski, *Adsorption* **2013**, 19, 423-434.
[44] G. Denuault, C. Milhano, D. Pletcher, *Phys. Chem. Chem. Phys*. **2005**, *7*, 3545–3551.
[45] M. S. Ahmed, S. Jeon, *J. Electrochem. Soc*. **2014**, *161*, F1300–F1306.
[46] Y. Feng, D. Bin, B. Yan, Y. Du, T. Majima, W. Zhou, *J. Colloid Inter. Sci.* **2017**, 493, 190-197.
[47] H. Rostami, T. Abdollahi, P. Mehdipour, A. A. Rostami, D. Farmanzadeh, *Int. J. Hydrogen Energy* **2017**, 42, 24713-24725.
[48] W. Huang, H. Wang, J. Zhou, J. Wang, P. N. Duchesne, D. Muir, P. Zheng, N. Han, F. Zhao, M. Zeng, J. Zhong, C. Jin, Y. Li, S. T. Lee, H. Dai, *Nature Commun.* **2015**, 1-8.
[49] L. Chen, L. Lu, H. Zhu, Y. Chen, Y. Huang, Y. Li, L. Wang, *Nature Commun.* **2017**, 1-8.
[50] http://www.casaxps.com/.
[51] R. I. Taylor, Phys. Rev. Lett. **1972**, *29*, 1088–1092.
[52] T. J. Cardwell, J. Mocaka, J. H. Santos, A. M. Bond, *Analyst* **1996**, *121*, 357-362.

Accepted Manuscript

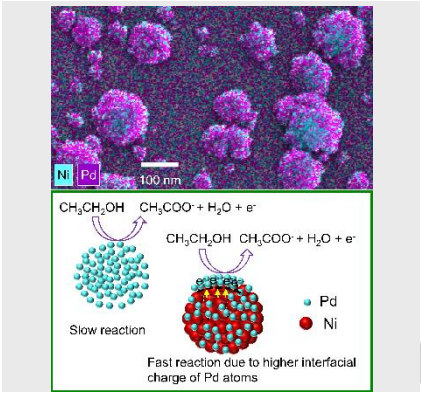
This article is protected by copyright. All rights reserved.

10.1002/celc.201701105

WILEY-VCH

ARTICLE

Electrochemical synthesis of bimetallic Pd-Ni nanoparticles on oxygen-terminated boron-doped diamond (BDD) substrate is described for use as electrocatalyst in direct ethanol fuel cell. The synthesised Pd-Ni nanoparticles shows 2.4 times higher mass activity compared to similar systems in literature owing to the enhanced synergistic effects of the electron interaction at the interfaces of two metals.



Dr. C. K. Mavrokefalos, Dr. M. Hasan, Dr. J. F. Rohan, Prof. J. S. Foord**

Page No. 1-11.

Enhanced Mass Activity and Stability of Bimetallic Pd-Ni Nanoparticles on Boron-Doped Diamond for Direct Ethanol Fuel Cell Applications

WILEY-VCH

Accepted Manuscript

This article is protected by copyright. All rights reserved.